Parametric dependencies of low-k turbulence in NSTX H-mode pedestals

D. R. Smith[1], R. J. Fonck[1], G. R. McKee[1], R. E. Bell[2], Y. Chen[3], A. Diallo[2], B. D. Dudson[4], S. M. Kaye[2], B. P. LeBlanc[2], R. Maingi[5], S. E. Parker[3], B. M. Stratton[2] and W. Wan[3]

[1]University of Wisconsin-Madison, Madison, WI, USA
[2]Princeton Plasma Physics Laboratory, Princeton, NJ, USA
[3]University of Colorado, Boulder, CO, USA
[4]University of York, York, UK
[5]Oak Ridge National Laboratory, Oak Ridge, TN, USA

Corresponding Author: drsmith@engr.wisc.edu

Abstract:

We present measurements and simulations of pedestal turbulence in ELM-free, MHD quiescent H-mode plasmas in the National Spherical Torus Experiment. Measurements indicate poloidal correlation lengths are $L_p/\rho_i \sim 10$, wavenumbers are $k_\theta \rho_i \sim 0.2$, and decorrelation times are $\tau_d/(a/c_s) \sim 5$. Parametric dependencies among turbulence quantities and plasma parameters indicate L_p increases and k_θ decreases at higher ∇n_e and lower ∇T_i. The parametric dependencies are most consistent with trapped-electron mode turbulence, partially consistent with kinetic ballooning mode and microtearing mode turbulence, and least consistent with ITG turbulence. Finally, we report on preliminary gyrokinetic and fluid simulations of NSTX pedestal turbulence. Growth rates from gyrokinetic simulations exhibit dependencies similar to measured correlation lengths, and correlation lengths and wavenumbers from a fluid simulation compare favorably to measured values.

1 Introduction

Global confinement predictions for ITER depend upon accurate physics models for the edge and pedestal regions. The spherical torus (ST) [1] parameter regime is notable for high β ($2\mu p/B^2$), large ρ^* (ρ_s/a), strong beam-driven flow, and strong shaping. Edge simulations in the ST parameter regime present a formidable validation challenge that compounds the inherent challenges of edge simulations. The need for valid edge and pedestal models for ITER and next-step devices motivates efforts to characterize low-k pedestal turbulence in the challenging ST parameter regime. Recent results from the National Spherical Torus Experiment (NSTX) [2] highlight the novel turbulence and transport properties of ST plasmas. For instance, stabilization or suppression of low-wavenumber (low-k) turbulence by strong equilibrium $E \times B$ flow shear [3] and field line curvature [4]

are leading explanations for near neoclassical ion thermal transport in NSTX beam-heated plasmas [5]. The high β regime makes ST plasmas more susceptible to low-k microtearing modes [6], and the scaling of NSTX confinement time with collisionality is consistent with collisional microtearing modes [7]. Also, turbulence measurements at the top of the H-mode pedestal during the ELM cycle are found to be consistent with ion-scale turbulence [8, 9].

Here, we characterize low-k pedestal turbulence quantities from beam emission spectroscopy measurements during ELM-free, MHD quiescent phases in NSTX H-mode discharges. In addition, we identify parametric dependencies among turbulence quantities and transport-relevant plasma parameters, and we provide preliminary comparisons between measurements and pedestal turbulence simulations. Turbulence measurements in Section 2 show poloidal correlation lengths in the pedestal are typically $L_p \approx 15$ cm and $L_p/\rho_i \approx 10$, and poloidal wavenumbers are typically $k_\theta \rho_i \approx 0.2$. The dimensionless quantities are are similar to measurements in the core regions of L-mode tokamak discharges [10] and consistent with drift-wave turbulence parameters. Parametric dependencies among turbulence quantities and plasma parameters in Section 3 indicate L_p increases and k_θ decreases at higher ∇n_e and lower ∇T_i. The parametric dependencies are most consistent with trapped-electron mode turbulence, partially consistent with kinetic ballooning mode and microtearing mode turbulence, and least consistent with ITG turbulence. Finally, Section 4 presents preliminary gyrokinetic and fluid simulations of NSTX pedestal turbulence.

2 Pedestal turbulence measurements in ELM-free, MHD quiescent H-mode plasmas

The beam emission spectroscopy (BES) system on NSTX [11] measures D_α emission ($n = 3 \rightarrow 2$, $\lambda_0 = 656.1$ nm) from deuterium heating beams [12] to study ion gyroscale fluctuations associated with low-k turbulence and instabilities. BES measurements are sensitive to plasma density fluctuations with $\delta I_{D\alpha}/I_{D\alpha} \approx (1/2)\,(\delta n/n)$ where $I_{D\alpha}$ is the beam D_α emission intensity, and n is the plasma density [12]. BES measurements on NSTX are sensitive to fluctuations with $k_\perp \rho_s \lesssim 1.5$ where $\rho_s \approx 0.5$–1.5 cm is the ion sound gyroradius. Poloidally-separated channels in the pedestal region at $r/a \approx 0.80$–0.95 can measure the poloidal correlation length L_p, decorrelation time τ_d, and poloidal wavenumber k_θ of low-k turbulence. Ref. [11] provides an example of BES pedestal turbulence measurements on NSTX and describes the measurement principles and channel layout.

ELM-free and MHD quiescent periods in NSTX H-mode discharges were identified to study low-k pedestal turbulence ($k_\theta \rho_i \sim 0.2$ and $0.8 < r/a < 0.95$). BES signals were frequency filtered to isolate 8-50 kHz components, the typical frequency range for observed broadband turbulence. Discharges with $B_{T0} = 0.45$ T, $I_p = 700$–900 kA, and lower single-null geometry were screened for ELM-free, MHD quiescent periods that persisted at least 200 ms. Turbulence parameters from BES measurements were averaged over 15–45 ms intervals. Figure 1 shows density profiles and histograms of turbulence quan-
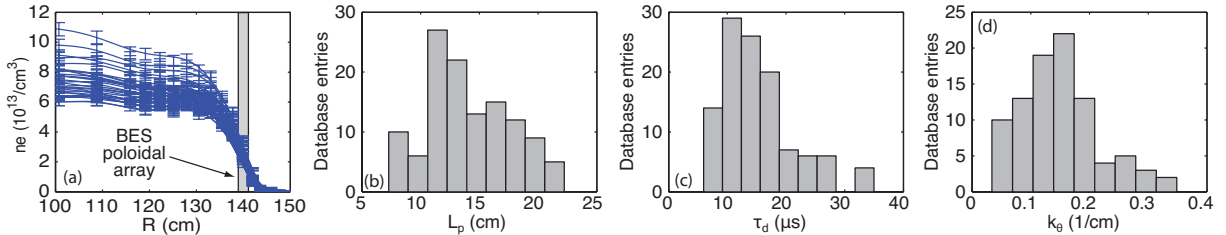
FIG. 1: (a) Density profiles for ELM-free, MHD quiescent discharges and BES measurement location (grey box); (b) histograms of poloidal correlation lengths, (c) decorrelation times, and (d) poloidal wavenumbers in the database.

tities in the H-mode database. Dimensionless turbulence quantities satisfy $L_p/\rho_i \sim 10$, $k_\theta \rho_i \sim 0.2$, and $\tau_d/(a/c_s) \sim 5$. Poloidal correlation lengths for low-field NSTX plasmas in the pedestal region are generally longer than previously reported correlation lengths in high-field tokamak plasmas [10], but dimensionless parameters like L_p/ρ_i and $\tau_d/(a/c_s)$ are similar. In addition to turbulence quantities, the database includes transport-relevant plasma parameters such as density and temperature gradients, collisionality, and β quantities. Plasma parameters in the database generally show 50%–300% variation. In the next Section, we untangle parametric dependencies among pedestal turbulence quantities and plasma parameters.

3 Parametric scalings of pedestal turbulence

Using measured turbulence quantities and plasma parameters, we now identify parametric dependencies using a stepwise multivariate linear regression (SMLR) algorithm and model aggregation [13]. Let y_i denote turbulence quantities such as correlation length, and let $x_{k,i}$ denote plasma parameters such as density gradient (i indexes database entry and k indexes plasma parameter). The SMLR algorithm finds models in the form

$$\frac{\hat{y}_i - \bar{y}}{\sigma_y} = \sum_k \alpha_k \frac{x_{k,i} - \bar{x}_k}{\sigma_k} \qquad (1)$$

where σ are standard deviations for y_i and $x_{k,i}$, and $\hat{y}_i$ are turbulence quantities predicted by the model. The α_k coefficients are the linear scaling coefficients when other plasma parameters in the model are fixed; parameters absent from the model are unconstrained. The SMLR algorithm minimizes the model's squared sum of errors, $SSE \equiv \sum_i (\hat{y}_i - y_i)^2$, by adding or removing x_k parameters such that the inferred significance of each α_k value exceeds 95% [14].

The SMLR algorithm searches the high dimensional x_k-space for regression models at SSE local minima. Many SSE local minima can exist, so the SMLR algorithm can find multiple final models by starting from different initial models. A single regression model provides a limited set of α_k scaling coefficients that are applicable only when other parameters in the model are fixed, and selecting the "best" model from a group of

models can be highly subjective due to numerous statistical metrics. Here, we implement a model aggregation technique appropriate for high dimensional datasets with complex interdependencies [13]. The model aggregation technique provides 1) α_k scalings for more plasma parameters than a single model can provide and 2) a distribution of α_k scalings for each plasma parameter under a variety of constraints.

Regression models identified by the SMLR algorithm are screened for multicollinearity and residual normality to ensure statistical validity. Multicollinearity is the linear dependence among regression variables (x_k), and excessive multicollinearity inflates the uncertainty of α_k coefficients [14]. Multicollinearity is assessed by limiting the cross-correlation among plasma parameter pairs in regression models and by limiting variance inflation factors VIF_k among model parameters [14]. Model aggregation results were consistent for cross-correlation limits in the range $C_{\text{limit}} = 0.5$–0.8, and only models with $\max(\text{VIF}_k) < 9$ were retained for analysis. Residual normality includes the independent and normal distribution of residuals ($r_i \equiv \hat{y}_i - y_i$) and absence of residual outliers. Non-normal residual distributions violate the mathematical framework of regression analysis. To assess residual normality, residuals are screened for outliers and the skewness and kurtosis of residual distributions are calculated. Studentized residuals, $r_i^s \equiv r_i/\sqrt{\text{var}(r_i)}$, follow a t-distribution, and models with $\max(|r_i^s|/t_{95}) > 1$, where t_{95} is the 95% significance level for the t-distribution, may contain outliers that distort the regression model. L_p and k_θ models exhibit $\max(|r_i^s|/t_{95}) < 1$ as desired, but some models for τ_d are marginal with $\max(|r_i^s|/t_{95}) \approx 1$. Skewness $\text{Sk} \equiv E(r_i - \bar{r})^3/\sigma_r^3$ and excess kurtosis $\text{Kt} \equiv E(r_i - \bar{r})^4/\sigma_r^4 - 3$ were calculated to assess the shape of the residual distribution. L_p models exhibit normal residual distributions within 2σ limits for skewness and kurtosis, but some k_θ models show skewness beyond the 2σ limit. In addition, τ_d models show skewness and kurtosis beyond the 2σ limits. The SMLR algorithm was initialized with about 8,000 parameter combinations, and the algorithm returned 9–50 models for each turbulence quantity, though different initial models often converged to the same final model. The coefficients of determination $R^2 \equiv \sum(\hat{y}_i - \bar{y})^2/\sum(y_i - \bar{y})^2$ indicate the models capture 50%–60% of the variation in the turbulence quantities [13].

We now identify parametric scalings that emerge from model aggregation. Figure 2 (a,c,e) shows α histograms for several parametric dependencies that emerge from model aggregation. $\alpha > 0$ ($\alpha < 0$) indicates the turbulence quantity increases (decreases) at higher parameter values. For example, Figure 2 (a) indicates 21 models for L_p contain a ∇n_e dependence, that is, $L_p \propto \alpha \nabla n_e$. The α coefficients cluster around $\alpha \approx 0.4$ despite different constraints and parameter combinations in each model. Collectively, the α coefficients from 21 models indicate L_p increases at higher ∇n_e for a variety of model scenarios. Figure 2(b) shows several parametric scalings for the turbulence quantities L_p, L_p/ρ_i, and L_p/ρ_s. Notably, the scalings are consistent for all normalizations of L_p. Figures 2(b-f) show similar results for k_θ and τ_d turbulence quantities. Also notable, parameter scalings common to L_p and k_θ are opposite in sign as expected because $L_p \sim 1/k_\theta$.

The random walk model for turbulent transport gives $D, \chi \sim L_r^2/\tau_d$ where L_r is the radial correlation length [15]. Assuming isotropic turbulence ($L_r \approx L_p$), the random walk model indicates turbulent transport increases at larger L_p and smaller τ_d. The quasi-linear
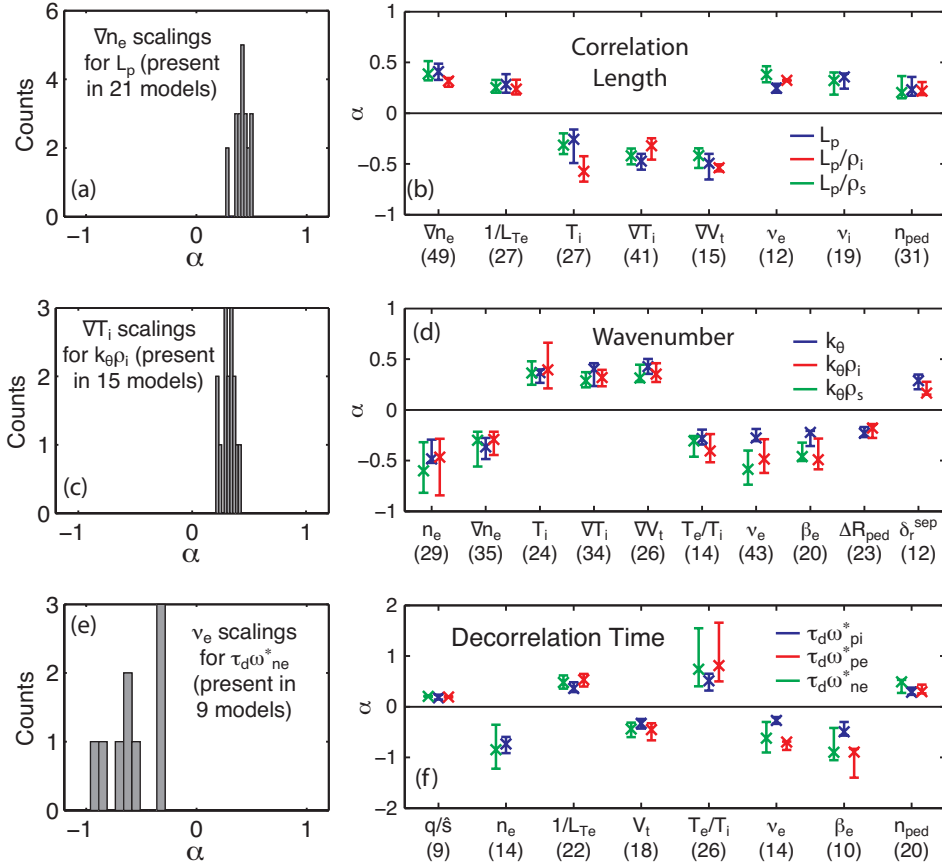
FIG. 2: (a) ∇n_e scalings for L_p and (b) parametric scalings from model aggregation for L_p. (c-f) are similar results for k_θ and τ_d quantities. Bars in (b,d,f) denote 10th-90th percentile limits; numbers below labels are the number of regression models.

model gives $D, \chi \sim (\gamma/k_\perp^2)_{\max k_\perp}$ where $k_\perp$ is the characteristic perpendicular wavenumber and γ is the linear growth rate. For stationary, isotropic turbulence ($k_\perp \sim L_p^{-1}$ and $\gamma \sim \tau_d^{-1}$), the quasi-linear model is consistent with the random walk model. Finally, nonlinear transport quantities take the form $D, \chi \propto \sum_{k_\theta} k_\theta |\tilde{\phi}(k_\theta)|^2$ where $\tilde{\phi}$ is the potential perturbation and fluctuation cross-phases are ignored. Turbulent spectra typically follow power laws like $|\tilde{\phi}(k_\theta)|^2 \sim k_\theta^{-\delta}$ with $\delta \approx 2$–4, so nonlinear transport models are consistent with random walk and quasi-linear models that give $D, \chi \sim 1/k_\theta^2 \sim L_p^2$. Collectively, turbulent transport models indicate larger L_p, smaller k_θ, and smaller τ_d enhance turbulent transport.

ITG turbulence is driven by ∇T_i, and ITG-driven transport is enhanced at larger T_e and T_e/T_i and smaller ν, T_i, and ∇n_e [16]. In Figure 2, we see the ∇T_i and ∇n_e scalings for L_p and k_θ are inconsistent with ITG-driven transport, and the ν scalings are similarly inconsistent. The T_e/T_i scalings for k_θ and τ_d show mixed agreement with ITG-driven transport. Disagreement with ∇T_i, ∇n_e, and ν scalings and mixed agreement for T_e/T_i scalings for ITG turbulence suggests the parametric scalings are not consistent with ITG-driven transport.

Trapped-electron mode (TEM) turbulence is driven by ∇n_e, and TEM-driven transport is enhanced at larger T_e/T_i and smaller ν and ∇T_e [17]. In Figure 2, we see the ∇n_e scalings for L_p and k_θ are consistent with TEM-driven transport, and the $1/L_{Te}$ scaling for τ_d is also consistent. The T_e/T_i scalings for k_θ and τ_d and the ν scalings show mixed agreement with TEM-driven transport. Agreement with ∇n_e and $1/L_{Te}$ scalings and mixed agreement for T_e/T_i and ν scalings points to TEM turbulence as a candidate mechanism for pedestal turbulence.

Kinetic ballooning mode (KBM) turbulence is driven by pressure gradients and exhibits a critical β_e value for onset [18]. The β_e scalings for k_θ and τ_d in Figure 2 are consistent with enhanced KBM-driven transport at higher β_e, but the ∇n_e, ∇T_i, and $1/L_{Te}$ scalings give mixed agreement in regard to KBM-driven transport. The partial agreement indicates KBM turbulence can be considered a candidate mechanism for pedestal turbulence.

Microtearing (MT) mode turbulence is driven by ∇T_e, and MT-driven transport is enhanced at higher ν_e and β_e [19]. All ν_e and β_e scalings in Figure 2 are consistent with enhanced MT-driven transport at higher ν_e and β_e. However, the $1/L_{Te}$ scaling for τ_d is inconsistent with MT-driven transport. Accordingly, MT turbulence can be considered a candidate mechanism based upon ν_e and β_e scalings. Note that nonlinear gyrokientic simulations in the NSTX core region in Ref. [19] indicate BES measurements will not be sensitive to MT turbulence with high k_r. However, linear gyrokinetic simulations of the NSTX pedestal (next section) indicate tearing parity instabilities are active.

In summary, parametric dependencies are most consistent with TEM turbulence, partially consistent with KBM and MT turbulence, and least consistent with ITG turbulence. Notably, recent turbulence measurements at the top of NSTX ELMy H-mode pedestals point to ITG turbulence [9]. The contradictory results may be due to measurement location (pedestal top vs. pedestal bottom) or H-mode scenario (ELMy vs. ELM-free).

4   Simulations of pedestal turbulence

The parametric dependencies identified in the previous section establish validation benchmarks for edge and pedestal turbulence simulations. Separatrix geometry and steep gradients are among the challenges for edge and pedestal turbulence simulations, and the spherical torus configuration introduces additional challenges with high β and large ρ^*. Preliminary gyrokinetic and fluid simulations of pedestal turbulence compare favorably with turbulence measurements and parametric dependencies described in the previous section.

We first consider BOUT++ fluid simulations [20] of NSTX pedestal turbulence. The 3D electromagnetic simulations implement a Braginskii fluid model [21] and evolve fluctuations on fixed background profiles. The simulations include collisions, $E \times B$ advection, field-line curvature, and drive terms for $J_\parallel$ and ∇P. The simulation radial domain typically spans $\psi_n \approx 0.85$ to 0.995. Figure 3 shows density fluctuations for an NSTX pedestal scenario, though not representative of typical plasma parameters in Section 3. Poloidal wavelengths are about 5–10 cm. Adjusting for pitch angle, fluctuations are $k_\theta \rho_i \sim 0.7$–1.4,
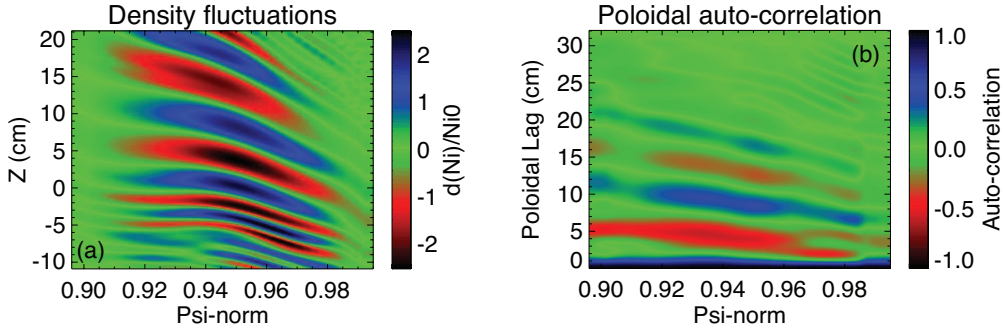
FIG. 3: BOUT++ Braginskii fluid simulation of an NSTX pedestal scenario: (a) density
fluctuations in the poloidal plane and (b) poloidal auto-correlation of density fluctuations.

so simulation wavenumbers are larger than measured wavenumbers. Poloidal correlation
lengths are $L_p/\rho_i \sim 8$, so simulation L_p values are consistent with measured L_p values. Taken together, correlation lengths and wavenumbers from the simulation compare
favorably with measured values.

Collisional electromagnetic gyrokinetic simulations of the pedestal region were performed for high and low ∇T_i and ∇n_e scenarios using the GEM code [22]. Preliminary
results indicate growth rates for intermediate n modes ($6 \leq n \leq 15$ and $k_\theta \rho_s \sim 0.2$) are
higher for high ∇n_e scenarios and lower for high ∇T_i scenarios. More specifically, 5 of
6 ∇n_e scenarios satisfied the growth rate pattern, and 7 of 7 ∇T_i scenarios satisfied the
growth rate pattern. In the framework of quasi-linear and random walk transport models,
the GEM results are consistent with measurements that show either longer correlation
lengths (or longer correlation times) at higher ∇n_e and lower ∇T_i. In most of the cases,
the instabilities are electromagnetic, destabilized by collisions and exhibit both ballooning
and tearing parity.

5   Summary

The ST parameter regime compounds the inherent challenges of edge/pedestal simulations and presents a difficult validation task. To advance validation efforts for edge and
pedestal models, we characterized NSTX pedestal turbulence using BES measurements
[11] in ELM-free, MHD quiescent H-mode plasmas. Normalized turbulence quantities are
consistent with generic low-k turbulence and previous measurements of tokamak L-mode
turbulence. Parametric dependencies among turbulence quantities and transport-relevant
plasma parameters are most consistent with trapped-electron mode turbulence, partially
consistent with kinetic ballooning mode and microtearing mode turbulence, and least
consistent with ITG turbulence. Finally, growth rates from GEM gyrokinetic simulations
exhibit dependencies similar to measured correlation lengths, and correlation lengths and
wavenumbers from a preliminary BOUT++ Braginskii fluid simulation compare favorably
with measured values.

References

[1] Y.-K. M. Peng. *Phys. Plasmas*, 7(5):1681, 2000.

[2] M. Ono, S. M. Kaye, Y.-K. M. Peng, et al. *Nucl. Fusion*, 40:557, 2000.

[3] M. Kotschenreuther, W. Dorland, Q. P. Liu, et al. *Nucl. Fusion*, 40:677, 2000.

[4] G. Rewoldt, W. M. Tang, S. Kaye, and J. Menard. *Phys. Plasmas*, 3:1667, 1996.

[5] S. Kaye et al. *Phys. Rev. Let.*, 98(17), 2007.

[6] K. L. Wong, S. Kaye, D. R. Mikkelsen, et al. *Phys. Plasmas*, 15(5):056108, 2008.

[7] W. Guttenfelder et al. *Phys. Rev. Let.*, 106:155004, 2011.

[8] A. Diallo, R.Maingi, S. Kubota, et al. *Nucl. Fusion*, 51:103031, 2011.

[9] A. Diallo et al. Progress in the characterization of the pedestal structure, stability and fluctuations during ELM cycle in NSTX. These proceedings, 2012.

[10] G. R. McKee et al. *Nucl. Fusion*, 41:1234, 2001.

[11] D. R. Smith et al. *Rev. Sci. Instrum.*, 83:10D502, 2012.

[12] R. J. Fonck, P. A. Duperrex, and S. F. Paul. *Rev. Sci. Instrum.*, 61(11):3487, 1990.

[13] D. R. Smith, R. J. Fonck, G. R. McKee, et al. Characterization and parametric dependencies of low wavenumber pedestal turbulence in the National Spherical Torus Experiment. Submitted for publication, 2012.

[14] M. Kutner, C. Nachtsheim, J. Neter, and W. Li. *Applied Linear Statistical Models*. McGraw-Hill, 5th edition, 2005.

[15] E. J. Doyle, W. A. Houlberg, Y. Kamada, et al. *Nucl. Fusion*, 47:S18, 2007.

[16] M. Kotschenreuther et al. *Phys. Plasmas*, 2:2381, 1995.

[17] J. Lang, Y. Chen, and S. E. Parker. *Phys. Plasmas*, 14:082315, 2007.

[18] P. B. Snyder and G. W. Hammett. *Phys. Plasmas*, 8:744, 2001.

[19] W. Guttenfelder et al. *Phys. Plasmas*, 19:022506, 2012.

[20] B. D. Dudson et al. *Comput. Phys. Commun.*, 180:1467, 2009.

[21] M. V. Umansky et al. *Comput. Phys. Commun.*, 180:887, 2009.

[22] Y. Chen and S. E. Parker. *J. Comput. Phys.*, 220:839, 2007.